THE JOURNAL OF PHYSICAL CHEMISTRY A
A JOURNAL OF THE AMERICAN CHEMICAL SOCIETY

pubs.acs.org/JPCA

Article

Minimum-Energy Conical Intersections by Compressed Multistate Pair-Density Functional Theory

Published as part of The Journal of Physical Chemistry A virtual special issue "Gregory A. Voth Festschrift".

Paul B. Calio, Matthew R. Hermes, Jie J. Bao, Ignacio Fdez. Galván, Roland Lindh, Donald G. Truhlar,* and Laura Gagliardi*

Cite This: *J. Phys. Chem. A* 2024, 128, 1698−1706

Read Online

ACCESS | Metrics & More | Article Recommendations | Supporting Information

ABSTRACT: Compressed multistate pair-density functional theory (CMS-PDFT) is a multistate version of multiconfiguration pair-density functional theory that can capture the correct topology of coupled potential energy surfaces (PESs) around conical intersections. In this work, we develop interstate coupling vectors (ISCs) for CMS-PDFT in the *OpenMolcas* and *PySCF/mrh* electronic structure packages. Yet, the main focus of this work is using ISCs to calculate minimum-energy conical intersections (MECIs) by CMS-PDFT. This is performed using the projected constrained optimization method in *OpenMolcas*, which uses ISCs to restrain the iterations to the conical intersection seam. We optimize the S_1/S_0 MECIs for ethylene, butadiene, and benzene and show that CMS-PDFT gives smooth PESs in the vicinities of the MECIs. Furthermore, the CMS-PDFT MECIs are in good agreement with the MECI calculated by the more expensive XMS-CASPT2 method.

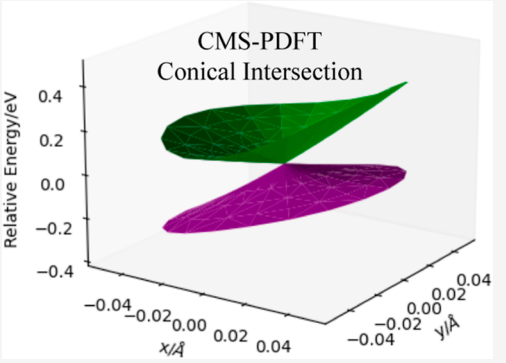

INTRODUCTION

Electronic nonadiabatic transitions are transitions in electronic states that preserve the electronic spin quantum number and are more likely to occur in regions where the coupling between adiabatic states is more pronounced. These regions can occur near conical intersections, which are multidimensional seams of molecular structures for which two adiabatic electronic states are degenerate.[1−15] When spin−orbit coupling may be neglected, conical intersections occur along $(F-2)$-dimensional seams, where F is the number of internal degrees of freedom (for polyatomic molecules, F equals $3N_{atoms}-6$, where N_{atoms} is the number of atoms). Understanding the energies and locations of conical intersections plays a pivotal role in unraveling the intricacies of photodynamics and UV−visible spectroscopy. Additionally, photoexcited molecules typically have enough energy to access a broad segment of the conical intersection seam, and the minimum-energy conical intersection (MECI, sometimes also called the minimum-energy crossing point) does not necessarily control the reaction rate or product distributions.[16] Nevertheless, an MECI identifies the minimum energy required to reach the crossing seam and frequently serves as the initial foundation for theoretical comprehension of photochemical reactions.

Accurate calculations of excited electronic states are challenging, and in many cases, a multiconfiguration wave function method is needed for useful accuracy.[17,18] Conical intersections are more challenging than typical vertical-excitation spectra, and wave functions at a conical intersection are intrinsically multiconfigurational. Multiconfiguration pair-density functional theory (MC-PDFT)[19−21] is a method that uses a multiconfiguration wave function as a reference and calculates the energy as a sum of the electronic kinetic energy, electron−nuclear attraction, classical electron−electron repulsion, and nonclassical energy that is computed from an on-top functional. MC-PDFT can be viewed as a multireference version of Kohn−Sham-DFT (KS-DFT), in which the Slater determinant is replaced by a multiconfiguration wave function and the exchange−correlation functional is replaced with an on-top density functional. Practical on-top density functionals may be obtained by translations of KS-DFT exchange−correlation functionals. MC-PDFT can calculate excitation energies as accurately as CASPT2 in many cases, but it has a significantly lower computational cost.[22] The state-averaged version of PDFT (SA-PDFT) uses a state-averaged complete-active-space self-consistent field (SA-CASSCF) wave function as the reference and is useful in regions far from conical intersections. However, SA-PDFT does not always calculate

Received: October 24, 2023
Revised: January 10, 2024
Accepted: January 31, 2024
Published: February 26, 2024

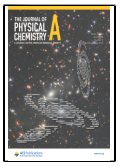

https://doi.org/10.1021/acs.jpca.3c07048
J. Phys. Chem. A 2024, 128, 1698−1706

excitation energies or potential energy surfaces correctly when potential energy surfaces (PESs) are close together.

Consistently achieving a PES with accurate topology at and in proximity to conical intersections demands an approach where all of the excited states are eigenvectors of the same effective Hamiltonian. Treatments with this feature are usually called quasi-degenerate, state-interaction, or multistate methods. Multistate PDFT methods[23−25] are extensions of MC-PDFT in which the final step is the diagonalization of an effective Hamiltonian in a set of intermediate states that span the same space as the SA-CASSCF states; this space is called the model space. Compressed multistate PDFT (CMS-PDFT)[25] is a special case of multistate PDFT in which the intermediate states are obtained by maximizing the classical electron−electron repulsion energy. The diagonal elements of the effective Hamiltonian in the CMS intermediate states are calculated by MC-PDFT, and the off-diagonal elements are calculated by a wave function method as in a conventional configuration interaction calculation. The CMS-PDFT method gives the correct topology of closely spaced PESs at and near conical intersections. CMS-PDFT may be compared to extended multistate complete active space second-order perturbation theory (XMS-CASPT2),[26,27] which has been demonstrated to be a highly accurate quantum chemical method that can describe important dynamic correlation effects at and near the conical intersections that control quenching and other electronically nonadiabatic processes.[28−35] Although CMS-PDFT gives results of comparable quality, including near conical intersections, it is advantageous as it is much less expensive.

This paper presents a method to find MECIs by CMS-PDFT and illustrates applications of this method to ethylene, butadiene, and benzene. As discussed in a recent review,[36] there are two kinds of algorithms used to find MECIs: those using the interstate coupling vector (ISC), **h**, and those not using **h**. Although **h** is not necessary to find MECIs, when they are available, "the efficiency of the optimization is substantially improved."[36] Because the use of **g** and **h** allows one to separate the intersection and branching subspaces, an algorithm that searches iteratively for the minimum energy on the seam can be more efficient if it uses **h** to restrain or constrain the iterations to the seam. The method presented in this article optimizes MECIs using the projected constrained optimization (PCO) with **g** and **h** as constraints,[37] as implemented in *OpenMolcas*.[38] The PCO method of ref 37 is an extension of the core PCO method explained in earlier papers.[39,40]

The new element needed for the present work is the calculation of the **h** vector. This calculation is similar to the calculation of analytic gradients and builds on our previous code for calculating gradients for single-state[41] and state-averaged[42,43] MC-PDFT and for CMS-PDFT.[44] In this work, we derive **h** for CMS-PDFT, and we implement it in the *OpenMolcas*[38,45−47] and *PySCF/mrh*[48,49] electronic structure software packages. We verify the **h** vector implementation by comparing the results between the two source codes (see Supporting Information). *OpenMolcas* is the only source code that has an MECI optimization algorithm via the PCO. The focus of this work is searching for MECI with CMS-PDFT and not implementing the PCO algorithm in electronic structure packages. Therefore, the results in this article will focus on CMS-PDFT MECI calculations using *OpenMolcas*. We compare our results to those obtained[50] with XMS-CASPT2 and two other variants of multistate CASPT2 (MS-CASPT2) and find excellent agreement.

The Theory section summarizes the CMS-PDFT energy calculation and provides the relevant equations characterizing the conical intersection. The Computational Methods section presents the details of our calculations. We next present the MECI for ethylene, butadiene, and benzene in the Results and Discussion section and then end with concluding remarks.

THEORY

CMS-PDFT involves four steps: (i) an SA-CASSCF calculation for n_{SA} states; (ii) the transformation of the SA-CASSCF eigenvectors to an intermediate basis that spans the same space (called the model space) as the SA-CASSCF eigenvectors but maximizes the classical electron−electron repulsion; (iii) the formation of an $n_{SA} \times n_{SA}$ model space Hamiltonian in the intermediate basis where the diagonal elements are obtained from an on-top density functional and the off-diagonal elements are formed by wave function theory as in a configuration interaction calculation; (iv) the diagonalization of the model-space Hamiltonian.

The intermediate states of step ii are the same as the diabatic states of the Edmiston-Ruedenberg method.[51,52] The eigenvalues of step iv are the CMS-PDFT approximations to the state energies; however, the corresponding eigenvectors are analogous to KS-DFT-optimized Slater determinants in that they do not directly reflect the physics of electron correlation that are modeled by the on-top density functional, and they should not be overinterpreted as proxies for eigenstates of the molecular Hamiltonian.

The results from step iv are used to calculate the ISC, **h**, whose derivation is similar to the derivation[44] of the nuclear gradients (see Supporting Information). The ISC, $\mathbf{h}_{MN}$, and the gradient difference vector, $\mathbf{g}_{MN}$, are used to search for and characterize the branching plane; they are defined as follows

$$\mathbf{g}_{MN} = \frac{1}{2}(\mathbf{g}_M - \mathbf{g}_N) \tag{1}$$

$$\mathbf{h}_{MN} = \frac{\mathrm{d}H_{MN}^{\mathrm{CMS}}(\lambda)}{\mathrm{d}\lambda} \tag{2}$$

where M and N denote the intersecting states, and $\boldsymbol{\lambda}$ is a $3N_{\mathrm{atoms}}$-dimensional vector of nuclear coordinates. The branching plane defines the tangent intersection space in which the degeneracy of a conical intersection is locally broken,[5,53−59] and the directions of $\mathbf{g}_{MN}$ and $\mathbf{h}_{MN}$ define the branching plane at a given point on the CI seam. In the CMS-PDFT method, M and N are the states that diagonalize the CMS-PDFT effective Hamiltonian matrix.

In *OpenMolcas*, orthonormal linear combinations of $\mathbf{h}_{MN}$ and $\mathbf{g}_{MN}$ are defined as follows[37]

$$\tilde{\mathbf{g}} = \mathbf{g}_{MN}\cos\beta + \mathbf{h}_{MN}\sin\beta \tag{3}$$

$$\tilde{\mathbf{h}} = \mathbf{g}_{MN}\cos\beta - \mathbf{h}_{MN}\sin\beta \tag{4}$$

$$\hat{\mathbf{x}} = \tilde{\mathbf{g}}/|\tilde{\mathbf{g}}| \tag{5}$$

$$\hat{\mathbf{y}} = \tilde{\mathbf{h}}/|\tilde{\mathbf{h}}| \tag{6}$$

where β is chosen to make the vectors orthogonal, and eqs 5 and 6 make them orthonormal. Geometries in the branching plane are then written as

https://doi.org/10.1021/acs.jpca.3c07048
J. Phys. Chem. A 2024, 128, 1698−1706

$$\boldsymbol{R}(x, y) = \boldsymbol{R}^{\times} + x\hat{\boldsymbol{x}} + y\hat{\boldsymbol{y}} \tag{7}$$

where $\boldsymbol{R}^{\times}$ is the geometry at the conical intersection. We can also convert these to polar coordinates

$$r = \sqrt{x^2 + y^2} \tag{8}$$

$$\theta = \arccos\left(\frac{x}{r}\right) = \arcsin\left(\frac{y}{r}\right) \tag{9}$$

Conical intersections are characterized using pitch (δ_{gh}), asymmetry (Δ_{gh}), relative tilt (σ), and tilt heading (θ_s), which are all functions of $\tilde{\mathbf{g}}$ and $\tilde{\mathbf{h}}$. The formulas for these derived functions are

$$\delta_{gh} = \sqrt{\frac{1}{2}(\tilde{\mathbf{g}}\cdot\tilde{\mathbf{g}} + \tilde{\mathbf{h}}\cdot\tilde{\mathbf{h}})} \tag{10}$$

$$\Delta_{gh} = \frac{\tilde{\mathbf{g}}\cdot\tilde{\mathbf{g}} - \tilde{\mathbf{h}}\cdot\tilde{\mathbf{h}}}{\tilde{\mathbf{g}}\cdot\tilde{\mathbf{g}} + \tilde{\mathbf{h}}\cdot\tilde{\mathbf{h}}} \tag{11}$$

$$\sigma = \sqrt{s_x^2 + s_x^2} \tag{12}$$

$$s_x = \frac{\boldsymbol{s}^{MN}\cdot\hat{\mathbf{x}}}{\delta_{gh}}; \qquad s_y = \frac{\boldsymbol{s}^{MN}\cdot\hat{\mathbf{y}}}{\delta_{gh}};$$

$$\mathbf{s}_{MN} = \frac{1}{2}(\mathbf{g}_M + \mathbf{g}_N) \tag{13}$$

$$\tan\theta_s = \frac{s_y}{s_x} \tag{14}$$

To simplify the conical intersection characterization, unitless parameters $\mathcal{P}$ and $\mathcal{B}$ are introduced to describe the PES of the higher and lower surfaces, which are functions of δ_{gh}, θ_s, Δ_{gh}, and θ. The equations for $\mathcal{P}$ and $\mathcal{B}$ are

$$\mathcal{P} = \frac{\sigma^2}{1 - \Delta_{gh}^2}(1 - \Delta_{gh}\cos(2\theta_s)) \begin{cases} < 1, \text{ peaked} \\ > 1, \text{ sloped} \end{cases} \tag{15}$$

$$\mathcal{B} = \sqrt[3]{\frac{\sigma^2}{4\Delta_{gh}^2}}\left(\sqrt[3]{(1 + \Delta_{gh})\cos^2\theta_s}\right)\left(\sqrt[3]{(1 - \Delta_{gh})\sin^2\theta_s}\right)$$
$$\begin{cases} < 1, & \text{bifurcating} \\ > 1, & \text{single path} \end{cases} \tag{16}$$

A $\mathcal{P}$ value less than 1 indicates that the conical intersection is a local-minimum-energy point of the upper surface, while a value greater than 1 indicates that the upper surface is tilted in such a way that its minimum-energy point is at a lower energy than the conical intersection. Intersections in these two classes are referred to as peaked and sloped intersections, respectively.

A $\mathcal{B}$ value greater than one indicates only a single local minimum along the path circling the intersection, and a $\mathcal{B}$ value less than one indicates multiple minima. Intersections in these two classes are called single-path intersections and bifurcating intersections, respectively. This classification may indicate whether the local topography of the surfaces favors decay from the conical intersection to one product or to more than one product, although a definitive conclusion about this would, in general, require consideration of permutational symmetry and nonadiabatic dynamics that take account of the shapes of the PESs beyond the linear region. Further discussion of the peak and bifurcation parameters is given in ref 59, and the original discussion along these lines was given by Atchity and Ruedenberg.[5]

Near the conical intersection, the upper and lower surfaces are linear in the polar coordinate r and are given by

$$E^{M}(r, \theta) = E^{\times} + \delta_{gh} r(\sigma\cos(\theta - \theta_s) + \sqrt{1 + \Delta_{gh}\cos 2\theta}) \tag{17a}$$

$$E^{N}(r, \theta) = E^{\times} + \delta_{gh} r(\sigma\cos(\theta - \theta_s) - \sqrt{1 + \Delta_{gh}\cos 2\theta}) \tag{17b}$$

where δ_{gh}, θ_s, Δ_{gh}, r, and θ are defined above, and $E^{\times}$ is the energy of the conical intersection. (One should not confuse the notation δ_{gh} used for the pitch with a Kronecker delta.) The MECI are further evaluated in this work by generating configurations in the branch plane using eq 7 and comparing their respective CMS-PDFT single-point energies with eq 17a (see Computational Methods for more details). Additionally, the presence of a conical intersection is confirmed by calculating the line integral of the wave function derivative coupling ($\mathbf{b}_{MN}$, see Supporting Information) in a closed circle around the MECI. A value of π verifies the presence of the conical intersection.[3,60,61] This line integral is equivalent to the following expression[37] (eq 18) and is used to evaluate the line integral in this work.

$$\oint \mathbf{b}_{MN}\cdot d\mathbf{R} = \int_0^{2\pi} b_{MN}^{\theta} d\theta$$
$$= \frac{1}{2}\sqrt{1 - \Delta_{gh}^2}\int_0^{2\pi} \frac{1}{1 + \Delta_{gh}\cos 2\theta} d\theta$$
$$= \pi \tag{18}$$

COMPUTATIONAL METHODS

CMS-PDFT ISCs are implemented into both *OpenMolcas* v23.02 (tag 466-g944b24d44) and *PySCF/mrh*. As numerical interstate coupling values are not readily available to compare with our analytical ISCs, we first check the CMS-PDFT interstate coupling implementation by comparing the results obtained with the two codes. The quantities we use to quantify the agreement between the codes are the mean unsigned difference (MUD), the norm of the average of the vectors ($\|AVG\|$), the norm of the difference of the vectors obtained with the two codes ($\|DIFF\|$), and the cos(θ) between the two vectors. We find good agreement between the two codes; as the focus of this paper is using CMS-PDFT to search for MECIs, we direct the reader to the Supporting Information for more details regarding the comparison.

We use the CMS-PDFT ISCs to compute MECI structures for ethylene, butadiene, and benzene with the PCO method[37,39,40] in *OpenMolcas*. We compare our results with the work of Nishimoto et al.,[50] who calculated S_1/S_0 MECI structures and conical intersections for various kinds of multistate CASPT2, including MS-CASPT2, XMS-CASPT2,[62] extended dynamically weighted (XDW-CASPT2),[63] and rotated multistate (RMS)-CASPT2.[64] Symmetry constraints were used neither in ref 50 nor in the CMS-PDFT calculations. The calculations of Nishimoto et al.[50] used the atomic compact Cholesky decomposition,[65,66] but this is not used in our CMS-PDFT gradient implementation. The Cholesky decomposition negligibly affects the results

https://doi.org/10.1021/acs.jpca.3c07048
J. Phys. Chem. A 2024, 128, 1698−1706

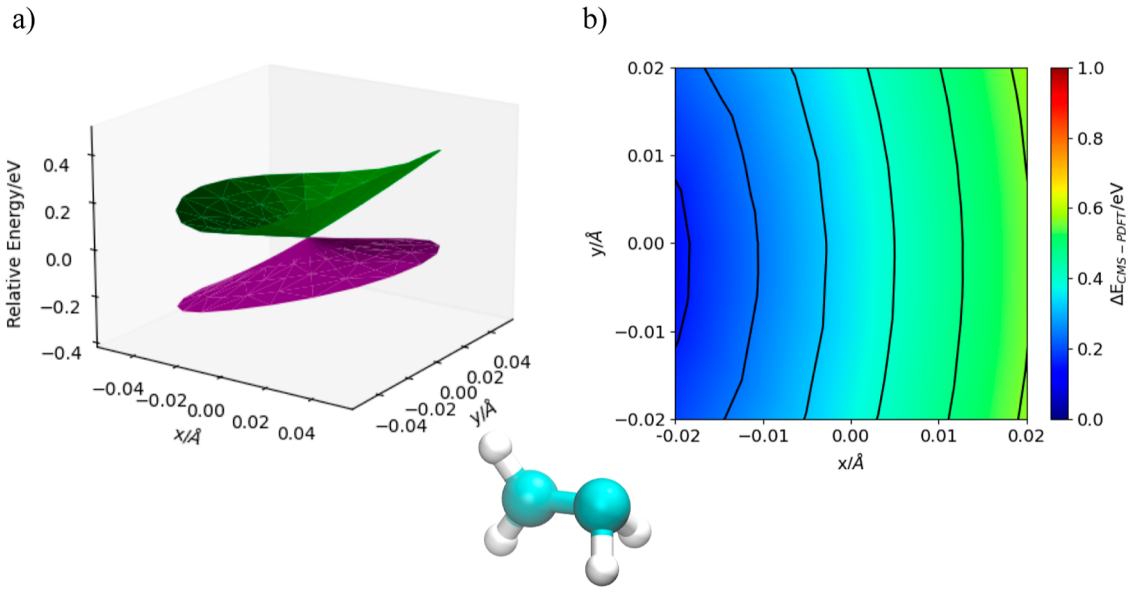

Figure 1. (a) CMS-PDFT PESs of the S_1 and S_0 electronic states of pyramidalized ethylene in the branching plane of the CMS-PDFT MECI. (b) CMS-PDFT energy difference between S_1 and S_0 in the branching plane of the SA-CASSCF MECI. The CMS-PDFT MECI geometry is depicted at the bottom.

and is used to decrease the computation cost of the two electron integrals.

The SA-CASSCF calculations for ethylene, butadiene, and benzene are averaged over three, two, and two states, respectively. The active space for ethylene includes 6 active electrons within 4 active orbitals (6e, 4o); that for butadiene was (4e, 4o), and that for benzene was (6e, 6o). To compare exactly with Nishimoto et al.,[50] ethylene and butadiene calculations used a cc-pVDZ basis set, and benzene calculations used a cc-pVTZ basis set. We note that, in general, a molecule may have multiple MECIs, and the calculated structures can depend significantly on details such as the number of averaged states and the active space size. See, for example, ref 37. Since the present work is not a complete study of the full conical intersection seams but rather a demonstration of a new method of locating MECIs, we limit our study to the structures found in the two-state calculations of Nishimoto et al.[50] The CMS-PDFT calculations used the tPBE on-top functional.[19−21,25] All optimizations used an ultrafine grid and no rotational invariance for the quadrature, and default threshold values were used for the SCF iterations, CMS intermediate-state iterations, and Lagrange multiplier solutions.

MECI calculations required the use of the SLAPAF module of *OpenMolcas* to update the structures during geometry optimizations. The tolerance in the SLAPAF optimization module of *OpenMolcas* was set equal to 10^{-5} au for all MECI optimizations. The initial geometries for optimizations of ethylene and butadiene are the XMS-CASPT2 MECI structures reported in the Supporting Information of ref 50, and the starting geometry for benzene is the XMS-CASPT2 MECI structure reported in the Supporting Information of ref 67.

Once MECI structures are optimized, geometries in the branching plane are generated according to eq 7, and single-point energy calculations for each structure are performed and compared to energies using eq 17a. The single-point energy calculations had tighter convergence thresholds for the SA-CASSCF and CMS intermediate state iterations by 1 order of magnitude. This meant that the SA-CASSCF energy, SA-CASSCF orbital rotation matrix, SA-CASSCF energy gradient, and the CMS intermediate-state thresholds were set to 10^{-9}, 10^{-5}, 10^{-5}, and 10^{-9} a. u., respectively.

Comparing the energies from eq 17a to the single-point energy calculations is used to validate the theoretical derivation and the accuracy of the implementation.

RESULTS AND DISCUSSION

An objective of ref 50 and the present work is to confirm the smoothness of the calculated PESs around the MECIs. This is motivated by the fact that MS-CASPT2 was shown to have unphysical behavior around conical intersections of the molecules in ref 50 due to the noninvariance with respect to unitary rotations among the reference states.[64,68,69] Nishimoto et al. showed discontinuities around the conical intersection in MS-CASPT2, while, for the most part, XMS-CASPT2, XDW-CASPT2, and RMS-CASPT2 have smooth PESs around their MECIs and around SA-CASSCF conical intersections.[50]

Ethylene. Figure 1 shows that the calculated PESs for pyramidalized ethylene are smooth both in the branching plane of the CMS-PDFT MECI and in the branching plane of the SA-CASSCF MECI. The PES around the conical intersection was generated using configurations that were five radial displacements from the conical intersection, each separated by 0.01 Å, and 20 structures angularly around the conical intersection.

Figure 2 compares the linear approximation of eq 17a to single-point energy calculations for pyramidalized ethylene. Since the linear approximations are calculated from nuclear gradients and ISCs, their agreement with single-point energies is a consistency check, and the figure shows that the check is well satisfied. The mean unsigned differences between these linear approximations and the single-point energies for the lower and upper electronic states are only 0.47 and 0.30 μE_h, respectively. We further apply the linear approximation to

https://doi.org/10.1021/acs.jpca.3c07048
J. Phys. Chem. A 2024, 128, 1698−1706

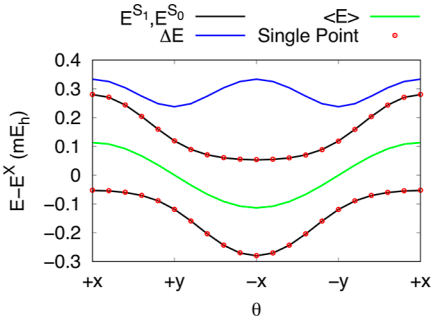

Figure 2. CMS-PDFT energies around the CMS-PDFT MECI for pyramidalized ethylene with r set to 0.001 Å. The black lines correspond to the first-order energies calculated according to eq 17a; the blue and green lines correspond to the energy difference and average energy, respectively, of the first-order energies. In red circles are single-point CMS-PDFT energies.

determine the line integral around the MECI according to eq 18, and we obtain 3.14159.

The $\mathcal{P}$ and $\mathcal{B}$ parameters for the CMS-PDFT MECI of pyramidalized ethylene are 0.46 and 1.26, respectively, which correspond to a peaked single-path conical intersection. This same character was found[50] with the XMS-CASPT2, XDW-CASPT2, and RMS-CASPT2 methods. The peaked single-path character of the conical intersection is illustrated in Figure 2, where the upper surface does not drop below the conical intersection (indicating a peaked intersection), and the lower surface has a single local minimum (indicating a single-path intersection).

Butadiene. We performed a similar analysis on *s-trans*-butadiene. Reference 50 showed that XMS-CASPT2 yields smooth potential energies around its MECI and has only small irregularities in the energy difference around the SA-CASSCF conical intersection. In Figure 3a, we show that the CMS-PDFT energies in the branching plane around the CMS-PDFT MECI are smooth, and in Figure 3b, we show that they are smooth in the vicinity of the SA-CASSCF MECI. CMS-PDFT and XMS-CASPT2 both use intermediate states that are unitary transformations of the reference states. For both methods, diagonalization of the Hamiltonian in the intermediate basis was successful in producing smooth PESs.

Figure 4 compares the CMS-PDFT first-order energy approximation to single-point energy calculations for *s-trans*-

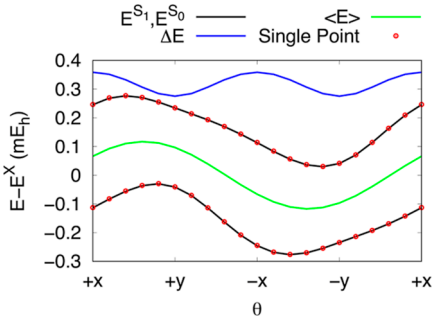

Figure 4. CMS-PDFT energies around the CMS-PDFT MECI for *s-trans*-butadiene with r set to 0.001 Å. Black lines are the first-order energies, and green and blue lines are the energy difference and average energy, respectively, of these approximate first-order energies. Red circles are single-point CMS-PDFT energies.

butadiene. As for ethylene, we notice agreement between the approximate and exact CMS-PDFT energies in black and red, respectively. The mean unsigned differences for the lower and upper states are 0.54 and 0.61 μE_H, respectively, and the line integral around the MECI according to eq 18 is 3.141593. The $\mathcal{P}$ and $\mathcal{B}$ parameters are 0.63 and 1.94, respectively, which indicates another peaked, single-path conical intersection. This is further illustrated in Figure 4, with the upper electronic surface not going below the conical intersection and the lower surface not having a single local minimum.

Benzene. There are several local minima on the conical intersection seam of benzene.[70] Previous work by spin-flip time-dependent DFT,[71] quasi-degenerate partially contracted n-electron valence state second-order perturbation theory (QD-PC-NEVPT2),[50] and extended multiconfiguration quasi-degenerate perturbation theory (XMC-QDPT2)[67] iden-

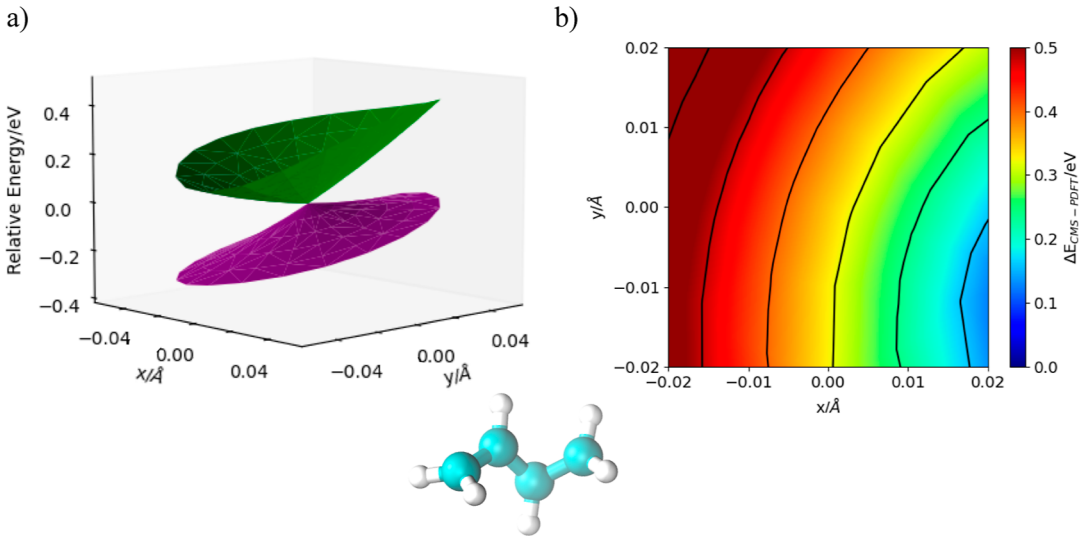

Figure 3. (a) CMS-PDFT PESs of the S_1 and S_0 electronic states of *s-trans*-butadiene in the branching plane of the CMS-PDFT MECI. (b) CMS-PDFT energy difference between S_1 and S_0 in the branching plane of the SA-CASSCF MECI. The CMS-PDFT MECI geometry is depicted at the bottom.

https://doi.org/10.1021/acs.jpca.3c07048
J. Phys. Chem. A 2024, 128, 1698−1706

tified eight such structures; however, one structure was found to be a saddle point in the intersection space[50] and was excluded from further analysis.[50,72] Here, we investigated the five lowest-energy structures of the remaining seven MECIs; following ref 67, these are labeled structures **1**−**4** and **6**. Figure 5 shows the relative energies of the MECIs for benzene relative

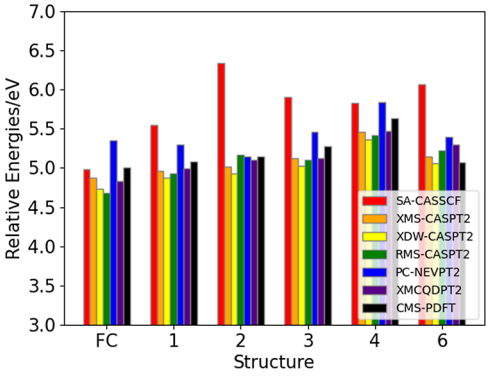

Figure 5. Relative energies for the structures of benzene. All energies are relative to the S_0 optimized ground state. FC denotes the vertically excited Franck−Condon point. SA-CASSCF (red), XMS-CASPT2 (orange), XDW-CASPT2 (yellow), and RMS-CASPT2 (green) values are from ref 50, PC-NEVPT2 (blue) values come from ref 67, XMCQDPT2 (purple) values are from ref 72, and black vlaue are the present CMS-PDFT results.

to the S_0 optimized ground state energy for SA-CASSCF, XMS-CASPT2,[62] XDW-CASPT2,[63] RMS-CASPT2,[64] QD-PC-NEVPT2,[67] XMCQDPT2,[72] and CMS-PDFT. We also show the S_1−S_0 vertical excitation energy at the Franck−Condon point. All relative energies are calculated for structures optimized with their respective methods. Using XMS-CASPT2 as the reference, all benzene MECI structures were found to be similar, as shown by an average root-mean-square deviation (rmsd) value less than 0.1 Å for all methods. (See Supporting Information).

The experimental Franck−Condon (FC) excitation energy is 4.9 eV,[73,74] and Figure 5 shows that CMS-PDFT predicts 5.0 eV, while XMS-CASPT2 predicts 4.97 eV. We therefore take the XMS-CASPT2 results as our best estimate for the MECI energies. Figure 5 shows good agreement (within ∼0.1 eV) of CMS-PDFT with XMS-CASPT2 for all five MECIs. Furthermore, the CASPT2 variants show structure **1** being more stable than structure **2**, which is more stable than structure **3**, and CMS-PDFT agrees with this energy ordering predicted by most of the multistate CASPT2 variants.

We further investigated benzene structure **4** in Figure 6 by showing the smooth PESs near CMS-PDFT's conical intersection (Figure 6a) and the smooth CMS-PDFT energy difference around SA-CASSCF's conical intersection (Figure 6b). The mean unsigned difference of the first-order energy curves in Figure 7 and the single-point energies are 0.80 and

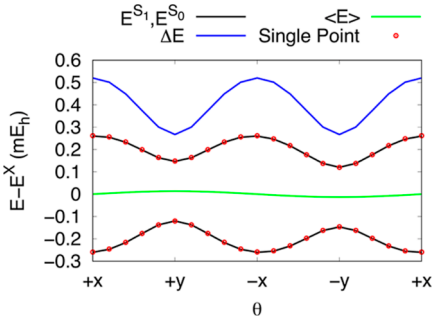

Figure 7. CMS-PDFT energies around the CMS-PDFT MECI for structure **4** of benzene with r set to 0.001 Å. Black lines are the first-order energies, and green and blue lines are the energy difference and average energy, respectively, of these approximate first-order energies. Red circles are single-point CMS-PDFT energies.

0.90 μE_H for the lower and upper surfaces, respectively. These MUDs are the same order of magnitude as for ethylene and butadiene. The low MUD in all three structures further verifies the accuracy of the ISC implementation in *OpenMolcas*. The line integral around the MECI according to eq 18 for structure

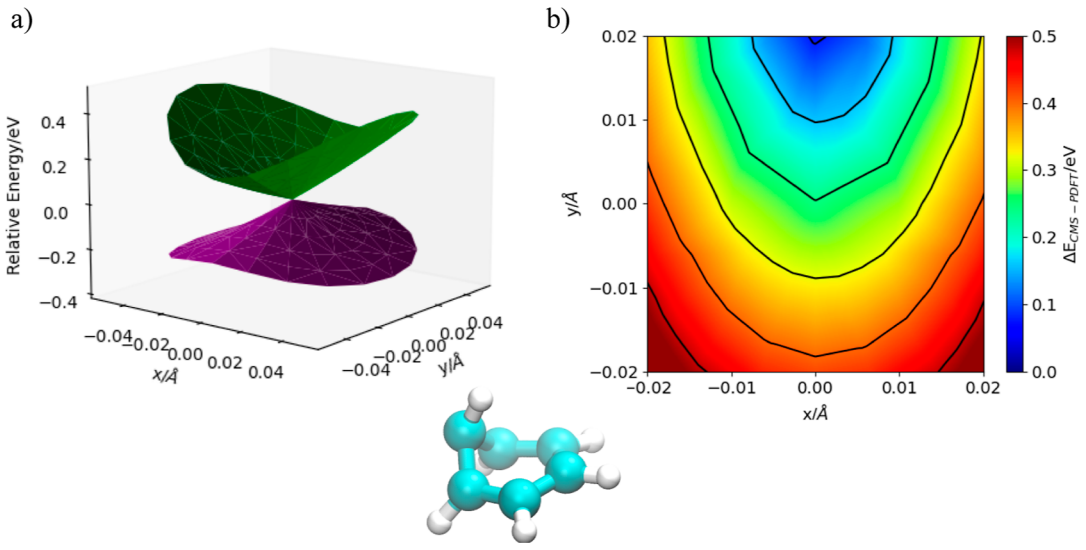

Figure 6. (a) CMS-PDFT PESs of the S_1 and S_0 electronic states of benzene MECI structure **4** in the branching plane of the CMS-PDFT MECI. (b) CMS-PDFT S_1 and S_0 energy differences in the branching plane of the SA-CASSCF MECI. The CMS-PDFT MECI geometry is depicted at the bottom.

https://doi.org/10.1021/acs.jpca.3c07048
J. Phys. Chem. A 2024, 128, 1698−1706

4 is 3.141593, and all other benzene structures also have a line integral of π. The CMS-PDFT's conical intersection corresponds to a peaked ($\mathcal{P}$ = 0.01) bifurcating ($\mathcal{B}$ = 0.11) conical intersection, which differs from the peaked single-path intersections present in the ethylene and butadiene molecules. The bifurcating lower PES can be seen in the two energy wells at + x and − x in the lower energy surface of Figure 7.

Structures. We calculated the root-mean squared distances (RMSDs) between the MECI structures for ethylene, butadiene, and benzene obtained by CMS-PDFT and those obtained by XMS-CASPT2. The RMSD is 0.20 Å for ethylene, 0.05 Å for butadiene, and 0.11 Å for benzene, and the RMSD for other CASPT2 variants relative to XMS-CASPT2 is given in the Supporting Information. The MECI-S_0 CMS-PDFT relative energy differences for ethylene and butadiene are 5.64 and 4.73 eV, respectively. In ref 50, Nishimoto et al. show that XMS-CASPT2, XDW-CASPT2, and RMS-CASPT2 show the S_1/S_0 MECI in ethylene at the same active space and basis set to be 4.555, 4.437, and 4.665 eV higher than the Franck−Condon point, respectively, but they do not report this value for butadiene. However, ref 72, using a cc-pVTZ basis set, shows the MECI-S_0 energy difference for butadiene to be 4.75 eV. The disagreement in the relative energies for ethylene is a result of different MECI structures (RMSD value of 0.20 Å), while the agreement in the relative energies for butadiene can be attributed to the better agreement between the MECI structures (RMSD value of 0.05 A). The difference between XMS-CASPT2 and CMS-PDFT is larger for ethylene than for butadiene or benzene. We note that this corresponds to a CMS-PDFT MECI structure with higher symmetry than that predicted by other methods—CMS-PDFT predicts a reflection plane along the carbon−carbon bond. (Symmetry was not enforced, and the calculation was not initialized from a high-symmetry geometry.) The carbon−carbon−hydrogen angles along the reflection plane are 102.1 and 100.3° (Figure 1), while XMS-CASPT2 breaks this reflection plane by creating carbon−carbon−hydrogen angles that are 82.5 and 115.6°. Of particular interest is the RMSD of benzene structure **4**, as the SA-CASSCF MECI structure differs significantly from the perturbation theory methods by having an RMSD value of 0.27 Å. The CMS-PDFT MECI structure **4** is in much better agreement with XMS-CASPT2, with a RMSD value of 0.03 Å, which is an order of magnitude smaller than SA-CASSCF.

CONCLUSIONS

We derived and implemented ISCs for CMS-PDFT. These ISCs are derived in a fashion similar to the analytic nuclear gradients for CMS-PDFT, and they are implemented in both the *OpenMolcas* and *PySCF/mrh* electronic structure packages. We checked the present implementation by comparing the agreement between the two codes, and we found good agreement (Supporting Information). However, the focus of this paper is the use of CMS-PDFT to search for MECIs. MECI optimizations were performed with routines already present in *OpenMolcas* for ethylene, butadiene, and benzene. We showed that CMS-PDFT provides smooth PESs around both the CMS-PDFT and CASSCF conical intersections. We compared our results with various multistate CASPT2 variants, and we observed that MECIs optimized with CMS-PDFT have energetics and characterizations similar to those obtained by multistate CASPT2 methods. In conclusion, CMS-PDFT is computationally less expensive than other post-SCF wave function methods for both energies and gradients, and the development of CMS-PDFT ISCs opens the door for efficient optimization of MECIs.

ASSOCIATED CONTENT

Supporting Information

The Supporting Information is available free of charge at https://pubs.acs.org/doi/10.1021/acs.jpca.3c07048.

CMS-PDFT notation for the derivative coupling and ISCs, CMS-PDFT theory and computational method for the calculation of the ISC, comparing results from *OpenMolcas* and *PySCF*, sample *OpenMolcas* input files, sample *PySCF* input files, Cartesian coordinates of the CMS-PDFT MECI optimized structures with absolute energies, and root-mean-square deviations of the MECI structures. A tar file containing *OpenMolcas* input and output files for the Frank-Condon and MECI optimizations is also present in the Supporting Information (PDF)

AUTHOR INFORMATION

Corresponding Authors

Donald G. Truhlar − *Department of Chemistry, Chemical Theory Center, and Minnesota Supercomputing Institute, University of Minnesota, Minneapolis, Minnesota 55455-0431, United States;* orcid.org/0000-0002-7742-7294; Email: truhlar@umn.edu

Laura Gagliardi − *Department of Chemistry, Pritzker School of Molecular Engineering, James Franck Institute, Chicago Center for Theoretical Chemistry, The University of Chicago, Chicago, Illinois 60637-1403, United States; Argonne National Laboratory, Lemont, Illinois 60439-4801, United States;* orcid.org/0000-0001-5227-1396; Email: lgagliardi@uchicago.edu

Authors

Paul B. Calio − *Department of Chemistry, Pritzker School of Molecular Engineering, James Franck Institute, Chicago Center for Theoretical Chemistry, The University of Chicago, Chicago, Illinois 60637-1403, United States;* orcid.org/0000-0001-8385-2628

Matthew R. Hermes − *Department of Chemistry, Pritzker School of Molecular Engineering, James Franck Institute, Chicago Center for Theoretical Chemistry, The University of Chicago, Chicago, Illinois 60637-1403, United States;* orcid.org/0000-0001-7807-2950

Jie J. Bao − *Department of Chemistry, Chemical Theory Center, and Minnesota Supercomputing Institute, University of Minnesota, Minneapolis, Minnesota 55455-0431, United States;* orcid.org/0000-0003-0197-3405

Ignacio Fdez. Galván − *Department of Chemistry-BMC, Uppsala University, Uppsala 75123, Sweden;* orcid.org/0000-0002-0684-7689

Roland Lindh − *Department of Chemistry-BMC, Uppsala University, Uppsala 75123, Sweden;* orcid.org/0000-0001-7567-8295

Complete contact information is available at: https://pubs.acs.org/10.1021/acs.jpca.3c07048

Notes

The authors declare no competing financial interest.

Published as part of *The Journal of Physical Chemistry A* virtual special issue "Gregory A. Voth Festschrift".

■ ACKNOWLEDGMENTS

The authors are grateful to Thais R. Scott, Matthew R. Hennefarth, and Yinan Shu for many helpful discussions. This work was supported by the National Science Foundation under grant CHE-2054723. The computational resources for this project were supported by the University of Chicago's Research Computing Center (RCC).

■ REFERENCES

(1) Teller, E. The Crossing of Potential Surfaces. *J. Phys. Chem.* **1937**, *41*, 109−116.
(2) Teller, E. Internal Conversion in Polyatomic Molecules. *Isr. J. Chem.* **1969**, *7*, 227−235.
(3) Herzberg, G. *Molecular Spectra and Molecular Structure. III. Electronic Spectra and Electronic Structure of Polyatomic Molecules*; Van Nostrand Reinhold: New York, 1966; p 442ff.
(4) Domcke, W.; Köppel, H.; Cederbaum, L. S. Spectroscopic Effects of Conical Intersections of Molecular Potential Energy Surfaces. *Mol. Phys.* **1981**, *43*, 851−875.
(5) Atchity, G. J.; Xantheas, S. S.; Ruedenberg, K. Potential Energy Surfaces Near Intersections. *J. Chem. Phys.* **1991**, *95*, 1862−1876.
(6) Robb, M. A.; Bernardi, F.; Olivucci, M. Conical intersections as a mechanistic feature of organic photochemistry. *Pure Appl. Chem.* **1995**, *67*, 783−789.
(7) Truhlar, D. G.; Mead, C. A. Relative Likelihood of Encountering Conical Intersections and Avoided Intersections on the Potential Energy Surfaces of Polyatomic Molecules. *Phys. Rev. A* **2003**, *68*, 032501.
(8) Worth, G. A.; Cederbaum, L. S. Beyond Born-Oppenheimer: Molecular Dynamics Through a Conical Intersection. *Annu. Rev. Phys. Chem.* **2004**, *55*, 127−158.
(9) Jasper, A. W.; Kendrick, B. K.; Mead, C. A.; Truhlar, D. G. Non-Born-Oppenheimer Chemistry: Potential Surfaces, Couplings, and Dynamics. In *Modern Trends in Chemical Reaction Dynamics Experiment and Theory (Part 1)*; Yang, X., Liu, K., Eds.; World Scientific: River Edge, NJ, 2004; pp 322−391.
(10) Malhado, J. P.; Bearpark, M. J.; Hynes, J. T. Non-adiabatic dynamics close to conical intersections and the surface hopping perspective. *Front. Chem.* **2014**, *2*, 97.
(11) Tuna, D.; Sobolewski, A. L.; Domcke, W. Electronically excited states and photochemical reaction mechanisms of *β*-glucose. *Phys. Chem. Chem. Phys.* **2014**, *16*, 38−47.
(12) Zhu, X.; Yarkony, D. R. Non-adiabaticity: The Importance of Conical Intersections. *Mol. Phys.* **2016**, *114*, 1983−2013.
(13) Guo, H.; Yarkony, D. R. Accurate Nonadiabatic Dynamics. *Phys. Chem. Chem. Phys.* **2016**, *18*, 26335−26352.
(14) Hong, Y.; Yin, Z.; Guan, Y.; Zhang, Z.; Fu, B.; Zhang, D. H. Exclusive Neural Network Representation of the Quasi-Diabatic Hamiltonians including Conical Intersections. *J. Phys. Chem. Lett.* **2020**, *11*, 7552−7558.
(15) Matsika, S. Electronic Structure Methods for the Description of Nonadiabatic Effects and Conical Intersections. *Chem. Rev.* **2021**, *121*, 9407−9449.
(16) Truhlar, D. G. General Discussion. *Faraday Discuss.* **2004**, *127*, 242−243.
(17) González, L.; Escudero, D.; Serrano-Andrés, L. Progress and Challenges in the Calculation of Electronic Excited States. *ChemPhysChem* **2012**, *13*, 28−51.
(18) Lischka, H.; Nachtigallová, D.; Aquino, A. J. A.; Szalay, P. G.; Plasser, F.; Machado, F. B. C.; Barbatti, M. Multireference Approaches for Excited States of Molecules. *Chem. Rev.* **2018**, *118*, 7293−7361.
(19) Li Manni, G.; Carlson, R. K.; Luo, S.; Ma, D.; Olsen, J.; Truhlar, D. G.; Gagliardi, L. Multiconfiguration Pair-Density Functional Theory. *J. Chem. Theory Comput.* **2014**, *10*, 3669−3680.
(20) Gagliardi, L.; Truhlar, D. G.; Li Manni, G.; Carlson, R. K.; Hoyer, C. E.; Bao, J. L. Multiconfiguration Pair-Density Functional Theory: A New Way To Treat Strongly Correlated Systems. *Acc. Chem. Res.* **2017**, *50*, 66−73.
(21) Zhou, C.; Hermes, M. R.; Wu, D.; Bao, J. J.; Pandharkar, R.; King, D. S.; Zhang, D.; Scott, T. R.; Lykhin, A. O.; Gagliardi, L.; et al. Electronic Structure of Strongly Correlated Systems: Recent Developments in Multiconfiguration Pair-Density Functional Theory and Multiconfiguration Nonclassical-Energy Functional Theory. *Chem. Sci.* **2022**, *13*, 7685−7706 and one other.
(22) Ghosh, S.; Verma, P.; Cramer, C. J.; Gagliardi, L.; Truhlar, D. G. Combining Wave Function Methods with Density Functional Theory for Excited States. *Chem. Rev.* **2018**, *118*, 7249−7292.
(23) Sand, A. M.; Hoyer, C. E.; Truhlar, D. G.; Gagliardi, L. State-Interaction Pair-Density Functional Theory. *J. Chem. Phys.* **2018**, *149*, 024106.
(24) Bao, J. J.; Zhou, C.; Varga, Z.; Kanchanakungwankul, S.; Gagliardi, L.; Truhlar, D. G. Multi-State Pair-Density Functional Theory. *Faraday Discuss.* **2020**, *224*, 348−372.
(25) Bao, J. J.; Zhou, C.; Truhlar, D. G. Compressed-State Multistate Pair-Density Functional Theory. *J. Chem. Theory Comput.* **2020**, *16*, 7444−7452.
(26) Finley, J.; Malmqvist, P.-Å.; Roos, B. O.; Serrano-Andrés, L. The Multi-State CASPT2Method. *Chem. Phys. Lett.* **1998**, *288*, 299−306.
(27) Shiozaki, T.; Győrffy, W.; Celani, P.; Werner, H.-J. Communication: Extended Multi-State Complete Active Space Second-Order Perturbation Theory: Energy and Nuclear Gradients. *J. Chem. Phys.* **2011**, *135*, 08110.
(28) Zhang, J.; Peng, J.; Hu, D.; Lan, Z. Investigation of Nonadiabatic Dynamics in the Photolysis of Methyl Nitrate (CH3ONO2) by on-the-Fly Surface Hopping Simulation. *Phys. Chem. Chem. Phys.* **2021**, *23*, 25597−25611.
(29) Kalita, P.; Medhi, B.; Singh, H. K.; Bhattacharyya, H. P.; Gupt, N.; Sarma, M. Perturbing *π*-Clouds with Substituents to Study the Effects on Reaction Dynamics of gauche-1,3-Butadiene to Bicyclobutane Electrocyclization. *ChemPhysChem* **2023**, *24*, No. e202200727.
(30) Nomoto, A.; Inai, N.; Yanai, T.; Okuno, Y. Substituent and Solvent Effects on the Photoisomerization of Cinnamate Derivatives: An XMS-CASPT2 Study. *J. Phys. Chem. A* **2022**, *126* (4), 497−505.
(31) Karashima, S.; Humeniuk, A.; Glover, W. J.; Suzuki, T. Ultrafast Photoisomerization of Ethylene Studied Using Time-Resolved Extreme Ultraviolet Photoelectron Spectroscopy. *J. Phys. Chem. A* **2022**, *126*, 3873−3879.
(32) Segarra-Martí, J.; Tran, T.; Bearpark, M. J. 3-Methylation Alters Excited State Decay in Photoionised Uracil. *Phys. Chem. Chem. Phys.* **2022**, *24*, 27038−27046.
(33) Reiter, S.; Bäuml, L.; Hauer, J.; de Vivie-Riedle, R. Q-Band Relaxation in Chlorophyll: New Insights from Multireference Quantum Dynamics. *Phys. Chem. Chem. Phys.* **2022**, *24*, 27212−27223.
(34) Soulié, C.; Paterson, M. J. Multistate Electronic Quenching: Nonadiabatic Pathways in NO A $^2\Sigma^+$ + O_2 X $^3\Sigma^-_g$ Scattering. *J. Chem. Phys.* **2022**, *157*, 164304.
(35) Rao, A. G.; Schapiro, I. Photoisomerization of Phytochrome Chromophore Models: An XMS-CASPT2 Study. *Phys. Chem. Chem. Phys.* **2022**, *24*, 29393−29405.
(36) Park, J. W.; Al-Saadon, R.; Macleod, M. K.; Shiozaki, T.; Vlaisavljevich, B. Multireference Electron Correlation Methods: Journeys Along Potential Energy Surfaces. *Chem. Rev.* **2020**, *120*, 5878−5909.
(37) Fdez. Galván, I.; Delcey, M. G.; Pedersen, T. B.; Aquilante, F.; Lindh, R. Analytical State-Average Complete-Active-Space Self-Consistent Field Nonadiabatic Coupling Vectors: Implementation with Density-Fitted Two-Electron Integrals and Application to Conical Intersections. *J. Chem. Theory Comput.* **2016**, *12*, 3636−3653.
(38) Li Manni, G.; Fdez. Galván, I.; Alavi, A.; Aleotti, F.; Aquilante, F.; Autschbach, J.; Avagliano, D.; Baiardi, A.; Bao, J. J.; Battaglia, S.; et al. The OpenMolcas Web: A Community-Driven Approach to Advancing Computational Chemistry. *J. Chem. Theory Comput.* **2023**, *19*, 6833−6991.

https://doi.org/10.1021/acs.jpca.3c07048
J. Phys. Chem. A 2024, 128, 1698−1706

(39) Anglada, J. M.; Bofill, J. M. A Reduced-Restricted-Quasi-Newton-Raphson Method for Locating and Optimizing Energy Crossing Points Between Two Potential Energy Surfaces. *J. Comput. Chem.* **1997**, *18*, 992−1003.
(40) De Vico, L.; Olivucci, M.; Lindh, R. New General Tools for Constrained Geometry Optimizations. *J. Chem. Theory Comput.* **2005**, *1*, 1029−1037.
(41) Sand, A. M.; Hoyer, C. E.; Sharkas, K.; Kidder, K. M.; Lindh, R.; Truhlar, D. G.; Gagliardi, L. Analytic Gradients for Complete Active Space Pair-Density Functional Theory. *J. Chem. Theory Comput.* **2018**, *14*, 126−138.
(42) Scott, T. R.; Hermes, M. R.; Sand, A. M.; Oakley, M. S.; Truhlar, D. G.; Gagliardi, L. Analytic Gradients for State-Averaged Multiconfiguration Pair-Density Functional Theory. *J. Chem. Phys.* **2020**, *153*, 014106.
(43) Scott, T. R.; Oakley, M. S.; Hermes, M. R.; Sand, A. M.; Lindh, R.; Truhlar, D. G.; Gagliardi, L. Analytic Gradients for Multiconfiguration Pair-Density Functional Theory with Density Fitting: Development and Application to Geometry Optimization in the Ground and Excited States. *J. Chem. Phys.* **2021**, *154*, 074108.
(44) Bao, J. J.; Hermes, M. R.; Scott, T. R.; Sand, A. M.; Lindh, R.; Gagliardi, L.; Truhlar, D. G. Analytic Gradients for Compressed Multistate Pair-Density Functional Theory. *Mol. Phys.* **2022**, *120*, No. e2110534.
(45) Fdez. Galván, I.; Vacher, M.; Alavi, A.; Angeli, C.; Aquilante, F.; Autschbach, J.; Bao, J. J.; Bokarev, S. I.; Bogdanov, N. A.; Carlson, R. K.; et al. OpenMolcas: From Source Code to Insight. *J. Chem. Theory Comput.* **2019**, *15*, 5925−5964.
(46) Minnesota-Chicago OpenMolcas Homepage. https://comp.chem.umn.edu/openmolcas (accessed July 28, 2023).
(47) OpenMolcas. https://github.com/Molcas/OpenMolcas (accessed July 28, 2023).
(48) Sun, Q.; Zhang, X.; Banerjee, S.; Bao, P.; Barbry, M.; Blunt, N. S.; Bogdanov, N. A.; Booth, G. H.; Chen, J.; Cui, Z.-H.; Eriksen, J. J.; Gao, Y.; Guo, S.; Hermann, J.; Hermes, M. R.; Koh, K.; Koval, P.; Lehtola, S.; Li, Z.; Liu, J.; Mardirossian, N.; McClain, J. D.; Motta, M.; Mussard, B.; Pham, H. Q.; Pulkin, A.; Purwanto, W.; Robinson, P. J.; Ronca, E.; Sayfutyarova, E. R.; Scheurer, M.; Schurkus, H. F.; Smith, J. E. T.; Sun, C.; Sun, S.-N.; Upadhyay, S.; Wagner, L. K.; Wang, X.; White, A.; Whitfield, J. D.; Williamson, M. J.; Wouters, S.; Yang, J.; Yu, J. M.; Zhu, T.; Berkelbach, T. C.; Sharma, S.; Sokolov, A. Y.; Chan, G. K.-L. Recent developments in the PySCF program package. *J. Chem. Phys.* **2020**, *153*, 024109.
(49) Hermes, M. R. https://github.com/MatthewRHermes/mrh (accessed July 28, 2023).
(50) Nishimoto, Y.; Battaglia, S.; Lindh, R. Analytic First-Order Derivatives of (X)MS, XDW, and RMS Variants of the CASPT2 and RASPT2Methods. *J. Chem. Theory Comput.* **2022**, *18*, 4269−4281.
(51) Atchity, G. J.; Ruedenberg, K. Determination of Diabatic States Through Enforcement of Configurational Uniformity. *Theor. Chem. Acc.* **1997**, *97*, 47−58.
(52) Subotnik, J. E.; Vura-Weis, J.; Sodt, A. J.; Ratner, M. A. Predicting Accurate Electronic Excitation Transfer Rates via Marcus Theory with Boys or Edmiston-Ruedenberg Localized Diabatization. *J. Phys. Chem. A* **2010**, *114*, 8665−8675.
(53) Manaa, M. R.; Yarkony, D. R. On the Intersection of Two Potential Energy Surfaces of the Same Symmetry. Systematic Characterization Using a Lagrange Multiplier Constrained Procedure. *J. Chem. Phys.* **1993**, *99*, 5251−5256.
(54) Bearpark, M. J.; Robb, M. A.; Bernhard Schlegel, H. A Direct Method for the Location of the Lowest-Energy Point on a Potential Surface Crossing. *Chem. Phys. Lett.* **1994**, *223*, 269−274.
(55) Bernardi, F.; Olivucci, M.; Robb, M. A. Potential Energy Surface Crossings in Organic Photochemistry. *Chem. Soc. Rev.* **1996**, *25*, 321−328.
(56) Yarkony, D. R. Nuclear Dynamics Near Conical Intersections in the Adiabatic Representation: I. The Effects of Local Topography on Interstate Transitions. *J. Chem. Phys.* **2001**, *114*, 2601−2613.
(57) Mori, T.; Kato, S. Dynamic Electron Correlation Effect on Conical Intersections in Photochemical Ring-Opening Reaction of Cyclohexadiene: MS-CASPT2 Study. *Chem. Phys. Lett.* **2009**, *476*, 97−100.
(58) Levine, B. G.; Coe, J. D.; Martınez, T. J. Optimizing Conical Intersections Without Derivative Coupling Vectors: Application to Multistate Multireference Second-Order Perturbation Theory (MS-CASPT2). *J. Phys. Chem. B* **2008**, *112*, 405−413.
(59) Nikiforov, A.; Gamez, J. A.; Thiel, W.; Huix-Rotllant, M.; Filatov, M. Assessment of Approximate Computational Methods for Conical Intersections and Branching Plane Vectors in Organic Molecules. *J. Chem. Phys.* **2014**, *141*, 124122.
(60) Herzberg, G.; Longuet-Higgins, H. C. Intersection of Potential Energy Surfaces in polyatomic Molecules. *Discuss. Faraday Soc.* **1963**, *35*, 77−82.
(61) Mead, C. A.; Truhlar, D. G. On the Determination of Born-Oppenheimer Nuclear Motion Wave Functions Including Complications Due to Conical Intersections and Identical Nuclei. *J. Chem. Phys.* **1979**, *70*, 2284−2296.
(62) Granovsky, A. A. Extended Multi-Configuration Quasi-Degenerate Perturbation Theory: The New Approach to Multi-State Multi-Reference Perturbation Theory. *J. Chem. Phys.* **2011**, *134*, 214113.
(63) Battaglia, S.; Lindh, R. Extended Dynamically Weighted CASPT2: The Best of Two Worlds. *J. Chem. Theory Comput.* **2020**, *16*, 1555−1567.
(64) Battaglia, S.; Lindh, R. On the Role of Symmetry in XDW-CASPT2. *J. Chem. Phys.* **2021**, *154*, 034102.
(65) Aquilante, F.; Lindh, R.; Bondo Pedersen, T. Unbiased Auxiliary Basis Sets for Accurate Two-Electron Integral Approximations. *J. Chem. Phys.* **2007**, *127*, 114107.
(66) Aquilante, F.; Gagliardi, L.; Pedersen, T. B.; Lindh, R. Atomic Cholesky Decompositions: A Route to Unbiased Auxiliary Basis Sets for Density Fitting Approximation with Tunable Accuracy and Efficiency. *J. Chem. Phys.* **2009**, *130*, 154107.
(67) Nishimoto, Y. Locating Conical Intersections Using the Quasidegenerate Partially and Strongly Contracted NEVPT2Methods. *Chem. Phys. Lett.* **2020**, *744*, 137219.
(68) Gozem, S.; Melaccio, F.; Valentini, A.; Filatov, M.; Huix-Rotllant, M.; Ferré, N.; Frutos, L. M.; Angeli, C.; Krylov, A. I.; Granovsky, A. A.; et al. Shape of Multireference, Equation-of-Motion Coupled-Cluster, and Density Functional Theory Potential Energy Surfaces at a Conical Intersection. *J. Chem. Theory Comput.* **2014**, *10*, 3074−3084.
(69) Park, J. W.; Shiozaki, T. Analytical Derivative Coupling for Multistate CASPT2 Theory. *J. Chem. Theory Comput.* **2017**, *13*, 2561−2570.
(70) Li, Q.; Mendive-Tapia, D.; Paterson, M. J.; Migani, A.; Bearpark, M. J.; Robb, M. A.; Blancafort, L. A Global Picture of the S1/S0 Conical Intersection Seam of Benzene. *Chem. Phys.* **2010**, *377*, 60−65.
(71) Harabuchi, Y.; Taketsugu, T.; Maeda, S. Combined Gradient Projection/Single Component Artificial Force Induced Reaction (GP/SC-AFIR) Method for an Efficient Search of Minimum Energy Conical Intersection (MECI) Geometries. *Chem. Phys. Lett.* **2017**, *674*, 141−145.
(72) Park, J. W. Analytical First-Order Derivatives of Second-Order Extended Multiconfiguration Quasi-Degenerate Perturbation Theory (XMCQDPT2): Implementation and Application. *J. Chem. Theory Comput.* **2020**, *16*, 5562−5571.
(73) Lassettre, E. N.; Skerbele, A.; Dillon, M. A.; Ross, K. J. High-Resolution Study of Electron-Impact Spectra at Kinetic Energies between 33 and 100 eV and Scattering Angles to 16°. *J. Chem. Phys.* **1968**, *48*, 5066−5096.
(74) Hiraya, A.; Shobatake, K. Direct Absorption Spectra of Jet-Cooled Benzene in 130−260 nm. *J. Chem. Phys.* **1991**, *94*, 7700−7706.

https://doi.org/10.1021/acs.jpca.3c07048
J. Phys. Chem. A 2024, 128, 1698−1706